Semi-continuous release of Cordilleran Ice Sheet meltwater between 20,000–17,000 years ago

Paul S. Wilcox[1*], Michael C. Meyer[1], and Daniela Festi[2]

[1]Institute of Geology, University of Innsbruck, 6020 Innsbruck, Austria

[2]Department of Geoanalytics and Reference Collections, Geosphere Austria, 1030 Vienna, Austria

Abstract

Terrestrial evidence of ice-sheet meltwater events registered in marine records during the early Last Deglaciation, between ~20,000–17,000 years ago, are exceptionally rare. However, as they allow spatio-temporal ice-decay dynamics to be constrained, they are a valuable complement to marine records. Here, we highlight a novel terrestrial Cordilleran Ice Sheet meltwater archive in a karstified glacial outwash plain during the early Last Deglaciation, showing semi-continuous meltwater events throughout the entire interval.

Main

Although the Last Deglaciation (LD), between ~20,000–11,000 years ago (ka), was one of the largest and most rapid natural climate changes in Earth's recent history (1), the sequence of events driving global climate change during this time period remains elusive. While it is generally accepted that insolation played an important role in shaping climate during the LD (2, 3, 4), it is less clear what internal forcings were necessary to kick-start deglacial conditions during the early LD, between ~20–17 ka. One of the leading hypotheses involved exceptionally large ice-sheet meltwater pulses discharging into the North Atlantic, termed Heinrich events, which are linked with ocean circulation changes and a cascading series of global climate perturbations (5).

Recently, marine records retrieved in the Gulf of Alaska provided evidence that enormous ice-sheet meltwater events, termed Siku events, occurred in the Northeast Pacific, thereby mimicking North Atlantic Heinrich events (6). However, Siku events were found to occur ~1,300 years earlier than Heinrich events, possibly serving as a necessary precursor in the sequence of events driving global climate change during the early LD (6). Currently, four Siku events have been identified, with the earliest Siku event (Siku event 4) constrained to ~42–39.5 ka (6)

Due to the significance of the discovery of Siku events, it is essential to corroborate this finding in other regional proxy data, such as in terrestrial archives, to better constrain spatio-temporal ice-decay dynamics of the Cordilleran Ice Sheet (CIS). However, the most recent Siku event (Siku event 1), between ~18–17 ka, occurred during a period of expansive ice-sheet formation (Fig. 1) (7, 8) that erased >90% of terrestrial glacioclastic sediments in North America (9). To this end, no terrestrial proxies that capture CIS meltwater deposition during the early LD have yet been reported.

Here, we utilize clastic cave sediment from Devils Canopy Cave in southeastern Alaska (Fig. 1) to help identify CIS meltwater events. The cave is situated in a karstified glacial outwash plain of the former CIS, i.e. in a unique geomorphological setting providing subsurface sediment traps that were sheltered from the erosional forces of the CIS, yet capable of storing clastic sediments transported by high-energy discharge events. Importantly, the cave sediment (herein referred to as Devils Sequence) represents a sediment depositional sequence extending through the early LD between ~20–17 ka, offering an exceptionally rare view of ice-sheet dynamics during this time period.

Devils Sequence was discovered in Devils Canopy Room (DC Room) (Extended Data Fig. 1) and is composed of two units: normally graded fine/medium sand at the base and a diamicton at the top (Extended Data Figs. 2, 3). There is no evidence of an unconformity between the two units and the sequence contains no plant macroremains. Sediment cemented to the top of DC Room indicate that the room was, at one time, completely full of sediment, and subsequently eroded to its current state. Given that Devils Sequence is against the perimeter wall of DC Room, it appeared unaffected by the erosional activity that took place in the central portion of DC Room.

The current geomorphology of Devils Canopy Cave and positioning of DC Room prohibit active sediment deposition. First, there is no modern-day source of quartz-rich sand or diamicton in the immediate vicinity of Devils Canopy Cave, being located in a thickly vegetated karstic landscape (Extended Data Fig. 4) (10). Second, the modern-day stream (Extended Data Fig. 4) provides insufficient energy to transport sand-sized grains or larger, except possibly during exceptional flooding events. Third, DC Room is ~5 m above the modern-day cave stream, preventing sediment deposition even during exceptional flooding events. Fourth, the constricted and sinuous cave passageways leading to DC Room prevents gravity-fed colluvial sediment transport. We suggest the sediment must have been transported by water through a now sealed passage that connected DC Room to the surface (Extended Data Fig. 1) and that high-energy discharge events were required to flush quartz pebbles, together with other lithologies up to cobble-sized, into the cave chamber. There is currently no evidence of active water transport through the sealed passage. The sediments within DC Room are likely in their original state since the former passage was sealed and have not been redeposited since entering the cave system.

We suspect that sediment within Devils Canopy Cave was heavily influenced by CIS meltwater. The most recent stadial period when the CIS extended to the approximate location of Devils Canopy Cave was between ~20–15 ka (Fig. 2) (7, 8). This would explain the deposition of both the quartz-bearing sand and diamicton units as the CIS released large but variable amounts of sediment-laden meltwater. Stadial conditions is supported by (i) the absence of plant macroremains and (ii) low concentrations of pollen in Devils Sequence, indicating sparse vegetation in a tundra-like environment above the cave prior to ~14 ka, which is in line with other regional pollen-based proxy records (11, 12, 13).

We argue that CIS meltwater discharge and transport of proglacial sediment, through the now sealed passage into DC Room (Extended Data Figs. 1, 3), represents the only plausible way for the deposition of Devils Sequence. More specifically, we suggest that all sediment within Devils Sequence was derived from a proglacial fluvial outwash plain hydrodynamically-linked to the CIS because (i) we observe resetting of the optically stimulated luminescence (OSL) quartz signals in the environmental dose (De)distributions (Extended Data Tables 1, 2), implying sunlight exposure of sand-sized quartz grains during sediment transport and (ii) found pollen within Devils Sequence (Extended Data Figs. 5, 6). Both observations would be unlikely, if not impossible, if the cave was overridden and sealed by the CIS during deposition of Devils Sequence. Therefore, the different sediment units within Devils Sequence represent different stages of meltwater events as the CIS advanced towards the cave site. We suggest the sand unit (Extended Data Fig. 2) represents near-continuous deposition based on the numerous normally graded sand beds and lack of erosion features. The individual graded units are likely separated by horizons of non-deposition and, as such, might capture peak discharge periods occurring on annual to decadal timescales. Conversely, we suggest the diamicton unit represents more instantaneous sediment deposition based on clast size (up to 15 cm), poor sorting, and age reversal. As such, the diamicton may represent one or several meltwater events within close proximity to the ice-sheet.

Based on these sediment transport assumptions, the age model constrains the timing of the sand unit between ~20–17 ka, and the diamicton at ~17 ka (Extended Data Fig. 2; Extended Data Table 1). The timing of Devils Sequence between ~20–17 ka implies that meltwater was being released from the CIS near its maximum extent (~20–17 ka) in southeastern Alaska (Figs. 1, 2) (7, 8). Importantly, the timing of CIS meltwater release between ~20–17 ka is in excellent agreement with marine proxies in the Gulf of Alaska indicating increased meltwater influx, cooling sea surface temperatures, and ice-rafted debris between ~19–16.5 ka (Fig. 2) (6, 14, 15), representative of Siku event 1. The timing of ice-sheet meltwater influx also aligns remarkably well with the absence of fossilized bones in caves on Prince of Wales Island (Figs. 1, 2) (16), suggesting that meltwater influx into the caves, rather than ice-sheets sealing the caves (16), might have caused this gap in animal occupation and/or fossil preservation. Based on these (albeit initial) findings and correlations, we conjecture that CIS meltwater events could have been a ubiquitous feature in southeastern Alaska between ~20–17 ka. CIS meltwater over this time period implies increased atmospheric warming, coeval with the switch to a La Niña mean state at ~19 ka (Fig. 2) (17) bringing warm/dry conditions to southeastern Alaska (18).

We suggest that Siku event 1, which is characterized by the release of large amounts of CIS meltwater concurrent to the CIS being at or near its maximum extent with expansive marine-terminating portions, is best explained by a purge-type ice-sheet response (19). This glacial feedback mechanism involves warming atmospheric conditions driving increased CIS meltwater, resulting in reduced basal friction and short-lived CIS acceleration with concomitant discharge of ice-rafted debris. Devils Sequence provides direct terrestrial evidence that CIS meltwater was being released at or near its maximum extent, corroborating this interpretation.

If our interpretations of CIS meltwater hydrodynamics leading to the deposition of Devils Sequence is correct, new avenues for investigating the LD and the steps leading from full-glacial into interglacial conditions and associated ice-sheet/ocean feedback mechanism open up. We recommend that terrestrial records should be used in tandem with marine records for a more complete picture of CIS spatio-temporal dynamics for interpreting past climate during the early LD. Additionally, the possibility of glacial refugia on outer-islands of southeastern Alaska will need to be re-evaluated during the maximum extent of the CIS, with our data indicating ice-free conditions. Future work should focus on investigating other caves in the region containing sediment deposits similar to Devils Sequence (Extended Data Fig. 7), which will allow an expanded view of CIS spatio-temporal ice-decay dynamics.

Methods

Site location and sampling strategy

Sediments were retrieved from Devils Canopy Cave, located in the temperate rainforest of northcentral Prince of Wales Island (56.105º N, 133.256º W, 167 m a.s.l.) (Fig. 1), within the Heceta Limestone unit. The cave is found in a topographically flat part of the island. Devils Sequence was found ~30 m behind the main entrance in Devils Canopy Room and ~10 m below the modern-day surface drainage (Extended Data Fig. 4). Devils Sequence is located on the perimeter of the room, with sediment in the sequence extending to the ceiling. The lower ~70 cm of the sequence needed to be dug-out to expose the full vertical sequence of 160 cm. The top of the sequence begins at 0 cm. Grain size samples were collected every 5 cm throughout the sequence, while sediment for OSL dating was sampled at 9, 48, and 126 cm depth (Extended Data Fig. 2).

Age model

A time-depth model was created by linearly interpolating the sand unit and assuming instantaneous deposition of the diamicton unit. As there was an age reversal in the diamiction unit (Extended Data Fig. 2), we infer the older of the two ages (17.3 ka) reflects a limiting (minimum) constraint for this transition, and place this age at the border of the sand unit. Ages were extrapolated for the lowermost sand unit based on the sedimentation rate produced from the linear interpolation. We applied a constant error of 3.0 ka throughout the record which represents the maximum error of all OSL ages. This time-depth model is based on a series of simple yet plausible assumptions regarding sediment transport mechanism and ice sheet dynamics. The key assumptions include i) the normally graded sand unit was deposited in a semi-continuous fashion with individual graded beds resulting from consecutive peak glacial discharge events and ii) the diamicton was deposited as glacial discharge product (similar to the sand unit), but under highly intensified hydrodynamic conditions, probably due to the close proximity of the advancing Cordilleran Ice Sheet margin at a much later stage of the early LD. We interpret the graded sand unit to reflect continuous build-up of material transported by proglacial runoff from an ice sheet margin maybe several km to tens of km from the cave entrance, likely over the course of several centuries to millennia. Conversely, the overlying diamicton unit likely represents nearly instantaneous deposition based on the large clasts, poorly-sorted sediment, and age reversal. The diamiction may represent one or several meltwater events within close proximity to the ice-sheet. This inference of continuous (graded sand) overlain by instantaneous (diamicton) deposition underpins our choice of time-depth model. The alternative interpretation that the entire sediment unit was deposited in a geologically instantaneous event cannot be completely ruled out, but appears less likely considering the sedimentological evidence, morphological setting and topographic position of the cave and general considerations regarding ice sheet dynamics, as also outlined in the main text.

Grain size

Grain size analysis was carried out using laser diffractometry (Malvern Mastersizer 3000) on bulk samples. To aid sample disaggregation, ultrasonication of 40% was applied for 40 s. Only grain sizes < 2000 µm were used for the analyses even though cobbles were identified in the upper section of the sequence.

OSL dating

OSL dating was conducted on coarse-grained (150-180 µm) purified quartz extracts following standard procedures using a Risø DA20 TL/OSL reader (21, 22) and a modified

SAR protocol (23, 24; Supplementary material). OSL ages were calculated based on the assumption that during rapid sediment transport only partial exposure to sunlight occurred. Hence the minimum age model was used for equivalent dose estimation and final age estimation (25; Extended Data Tables 1, 2).

Pollen analyses

Pollen analyses was conducted on sediment leftover from the grain size analyses at 12 depths (Extended Data Fig. 5) and prepared according to standard procedure (26). Filtering bigger particles at 200 µm and the smallest at 7 µm was used. A marker pollen *Lycopodium clavatum* tablet was added for each sample (Batch n. 101023-231; 20408±543 (27)). Chemical treatment included HCl (10%), Acetolysis solution and HF (20%) treatment. The concentrated pollen was mounted in glycerine for microscopy observation at the optic microscope (Leica Dm 2500) at x400 magnification. For every sample the complete content of pollen, fern spores and non-pollen playnomorphs (i.e. algae and fungi spores) was identified and quantified. The *Pinus* diploxylon type was assigned to *Pinus* cf. *contorta* and *Picea* type to *Picea* cf. *sitchensis* based on pollen morphology and phytogeography. Pollen diagram was plotted with the software C2 (28). The residue samples fractions >200 µm were analysed at the stereomicroscope to verify the presence of plant macroremains but no remains were found.

Data Availability: Devils Sequence OSL and grain size data is available at NOAA: (https://www.ncei.noaa.gov/access/paleo-search/study/39563).

References

1. Denton, G.H. et al. The last glacial termination. *Science* **328**, 1652–1656 (2010).
2. Carlson, A.E. & Winsor, K. Northern Hemisphere ice-sheet responses to past climate warming. *Nat. Geosci.* **5**, 607–613 (2012).
3. Abe-Ouchi, A. et al. Insolation-driven 100,000-year glacial cycles and hysteresis of ice-sheet volume. *Nature* **500**, 190–193 (2013).
4. Robinson, A. & Goelzer, H. The importance of insolation changes for paleo ice sheet modelling. *Cryosphere* **8**, 1419–1428 (2014).
5. Broecker, W.S. Massive iceberg discharges as triggers for global climate change. *Nature* **372**, 421–424 (1994).
6. Walczak, M.H. et al. Phasing of millennial-scale climate variability in the Pacific and Atlantic Oceans. *Science* **370**, 716–720 (2020).
7. Lesnek, A.J., Briner, J.P., Baichtal, J.F. & Lyles, A.S. New constraints on the last deglaciation of the Cordilleran Ice Sheet in coastal Southeast Alaska. *Quat. Res.* **96**, 140–160 (2020).
8. Dalton, A.S. et al. Deglaciation of the North American ice sheet complex in calendar years based on a comprehensive database of chronological data: NADI-1. *Quat. Sci. Rev.* **321**, 108345 (2023).
9. Eyles, N. The role of meltwater in glacial processes. *Sediment. Geol.* **190**, 257–268 (2006).
10. Wilson, F.H., Hults, C.P., Mull, C.G. & Karl, S.M. *Geol. Surv. Sci. Investig. Map* **3340**, 197 (2015).
11. Hansen, B.C. & Engstrom, D.R. Vegetation history of Pleasant Island, southeastern Alaska, since 13,000 yr BP. *Quat. Res.* **46**, 161–175 (1996).

12. Wilcox, P.S., Fowell, S.J. & Baichtal, J.F. A mild Younger Dryas recorded in southeastern Alaska. *Arct. Antarct. Alp. Res.* **52**, 236–247 (2020).
13. Lacourse, T., Mathewes, R.W. & Fedje, D.W. Late-glacial vegetation dynamics of the Queen Charlotte Islands and adjacent continental shelf, British Columbia, Canada. *Palaeogeogr. Palaeoclimatol. Palaeoecol.* 226, 36–57 (2005).
14. Praetorius, S.K. et al. The role of Northeast Pacific meltwater events in deglacial climate change. *Sci. Adv.* **6**, p.eaay2915 (2020).
15. Cowan, E.A. et al. Sediment controls dynamic behavior of a Cordilleran Ice Stream at the Last Glacial Maximum. *Nat. Commun.* **11**, 1826 (2020).
16. Lesnek, A.J., Briner, J.P., Lindqvist, C., Baichtal, J.F. & Heaton, T.H. Deglaciation of the Pacific coastal corridor directly preceded the human colonization of the Americas. *Sci. Adv.* **4**, p.eaar5040 (2018).
17. Wilcox, P.S., Spötl, C., Honkonen, J. & Edwards, R.L. A Walker switch mechanism driving millennial-scale climate variability. *Innov. Geo.* **1**, 100026 (2023).
18. Zhang, S. et al. Thermal coupling of the Indo-Pacific warm pool and Southern Ocean over the past 30,000 years. *Nat. Commun.* **13**, 5457 (2022).
19. MacAyeal, D.R. Binge/purge oscillations of the Laurentide ice sheet as a cause of the North Atlantic's Heinrich events. *Paleoceanography* **8**, 775–784 (1993).
20. Berger, A. Long-term variations of daily insolation and Quaternary climatic changes. *J. Atmos. Sci.* **35**, 2362–2367 (1978).
21. Bøtter-Jensen, L., Andersen, C.E., Duller, G.A. & Murray, A.S. Developments in radiation, stimulation and observation facilities in luminescence measurements. *Radiat. Meas.* **37**, 535–541 (2003).
22. Murray, A. et al. Optically stimulated luminescence dating using quartz. *Nat. Rev. Methods Primers* **1**, 72 (2021).

23. Murray, A.S. & Wintle, A.G. Luminescence dating of quartz using an improved single-aliquot regenerative-dose protocol. *Radiat. Meas.* 32, 57–73 (2000).

24. Cunningham, A.C. & Wallinga, J. Selection of integration time intervals for quartz OSL decay curves. *Quat. Geochronol.* **5**, 657–666 (2010).

25. Galbraith, R.F., Roberts, R.G., Laslett, G.M., Yoshida, H. & Olley, J.M. Optical dating of single and multiple grains of quartz from Jinmium rock shelter, northern Australia: Part I, experimental design and statistical models. *Archaeometry* **41**, 339–364 (1999).

26. Iversen, J. *Textbook of pollen analysis* (J. Wiley & Sons, 1989).

27. Stockmarr, J. Tables with spores used in absolute pollen analysis. *Pollen et spores* **13**, 615–621 (1971).

28. Juggins, S. C2 Data Analysis vs. 1.4.2 (1991).

Corresponding author wilcox214@gmail.com

Acknowledgments This work was funded by the Austrian Science Fund (FWF) grant FP338960. We are grateful to Anna Harris, Jim Baichtal, Christian DeCelle, and the Tongass National Forest Geology program for their continued support for this work. Additionally, we thank Jessica Honkonen for the invaluable field work assistance and Tatyana Ivanova for precious support in pollen samples preparation. Finally, we thank Christoph Spötl and Jeffrey Monroe for providing valuable feedback from an earlier version of this manuscript.

Author contributions: Conceptualized: P.S.W.; Funding acquisition: P.S.W.; Administered/supervised the project: P.S.W.; Methodology design: P.S.W.; Conducted OSL dating: M.C.M; Conducted pollen analysis: D.F; Prepared visual components: P.S.W., M.C.M.; Writing–original draft: P.S.W.; Writing–reviewing and editing: P.S.W, M.C.M., D.F.

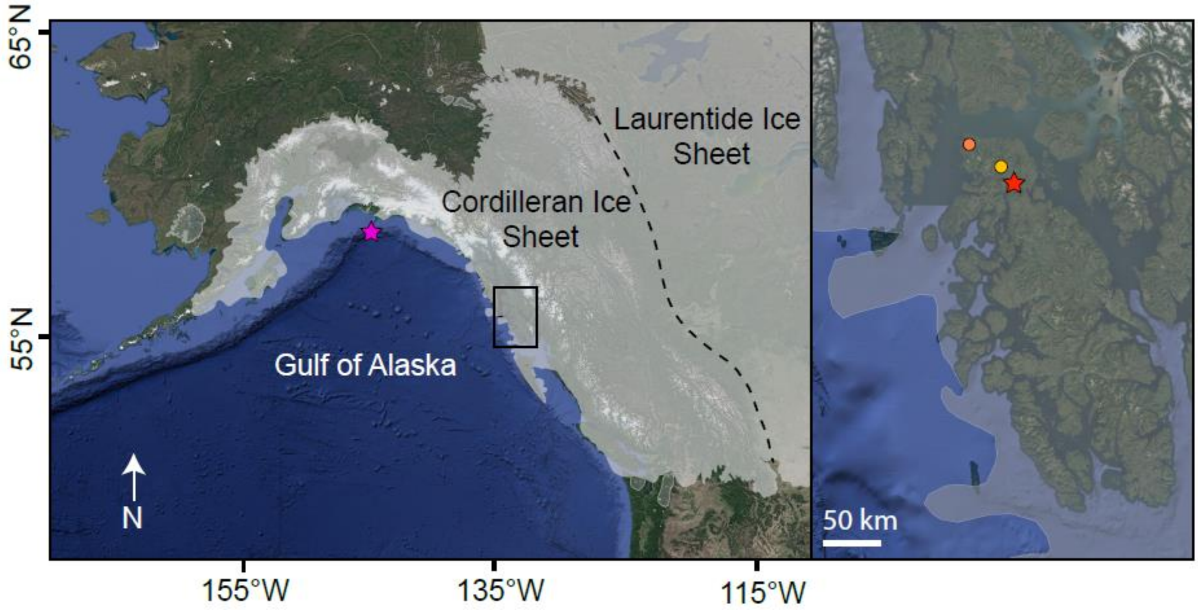

Fig. 1: Map of northwestern North America with optimal ice-sheet extent at 18 ka (8), with purple star marking sites U1419 (where Siku events were originally identified (6)) and U1421 (15). Map insert shows location of Devils Canopy Cave (this study) (red star) as well as El Capitan Cave (yellow circle) and Shuká Káa Cave (orange circle), where fossilized bones were found (16). Reconstructed CIS extend does not change significantly during the deposition of Devils Sequence (between ~20–17 ka) (8). Map data: Google Earth using WGS 84/Pseudo-Mercator projection.

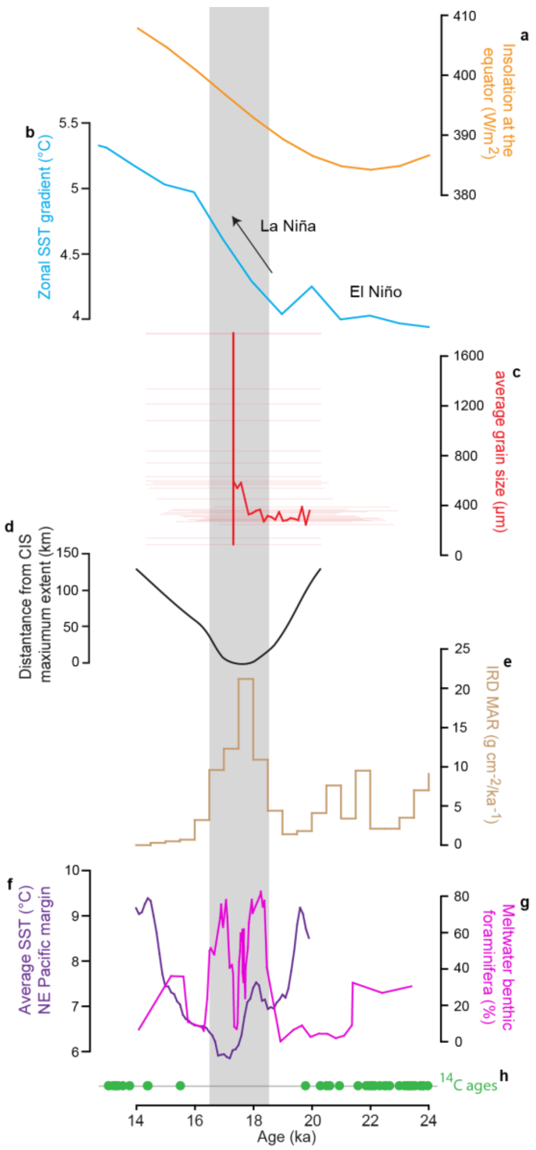

Fig. 2: Proxy comparisons. (**a**) June insolation at the equator (20). (**b**) Tropical Pacific SST index (18). (**c**) Devils Sequence sediment grain size (this study). (**d**) Approximate CIS configuration based on location/age of ^{10}Be of erratics, modified from Lesnek et al. (7). (**e**) Ice-rafted debris from the Gulf of Alaska at site U1419 (6). (**f**) Average sea surface temperatures (SST) from the Gulf of Alaska (14). (**g**) Percentage of benthic foraminifera (running average applied) indicative of meltwater from the Gulf of Alaska at site U1421 (15). (**h**) Calibrated ^{14}C ages from cave fauna (16). Fauna ^{14}C ages were omitted if errors were >1000 years. Gray bar denotes timing of Siku event 1.

Extended Data Figs. 1 – 7

Extended Data Table 1

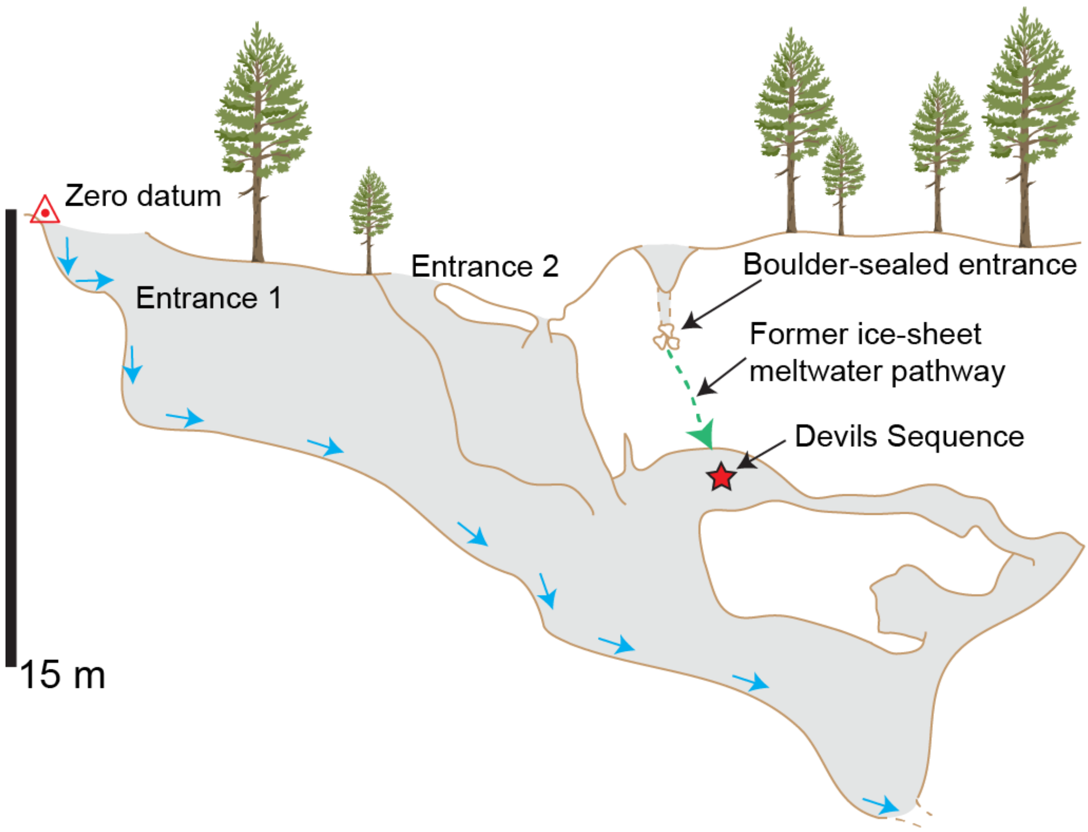

Extended Data Fig. 1: Profile map of Devils Canopy Cave. Blue arrows denote modern-day streamflow. Water from modern-day stream exits Devils Canopy into a large network of other caves, some being unexplored. Red star denotes location of Devils sequence in Devils Canopy Room. Also shown is the boulder-sealed passage where sediments from Devils Sequence are hypothesized to have originated before being blocked. Green dashed arrow shows possible pathway of former sediment-laden ice-sheet meltwater in DC Room. Map modified from original map by Kevin and Carlene Allred.

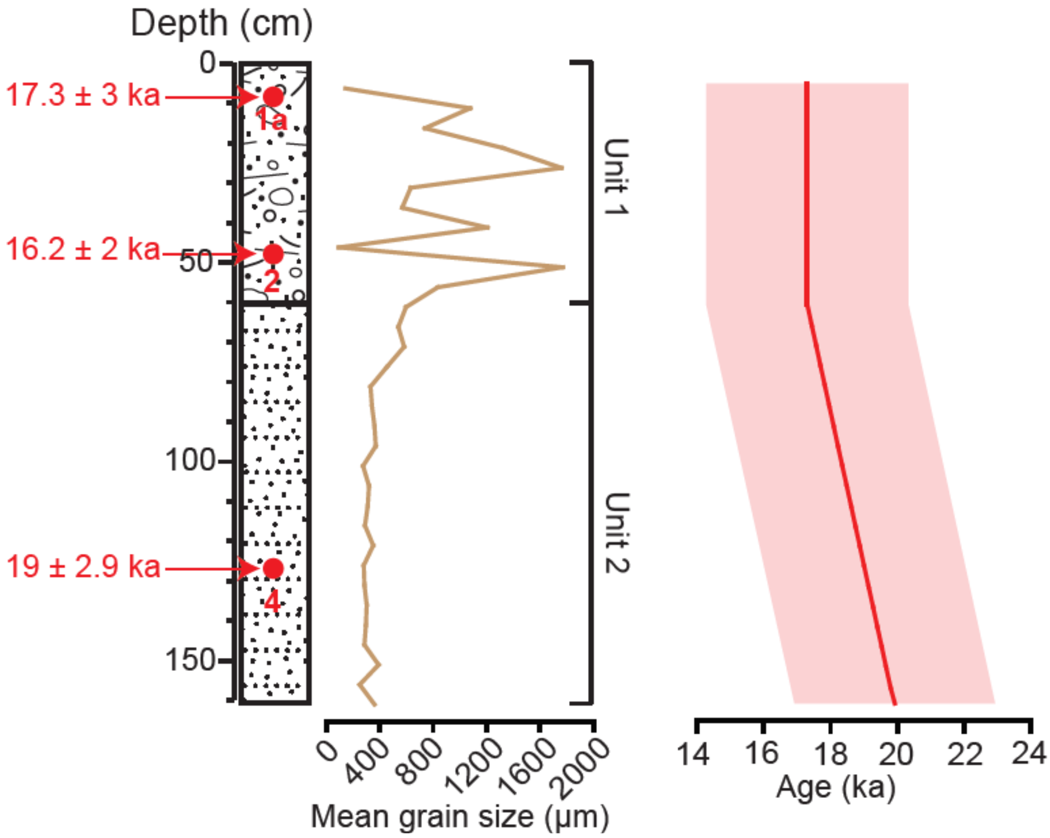

Extended Data Fig. 2: Illustration of Devils Sequence from Devils Canopy Cave. Unit 1 is composed of diamicton while unit 2 is composed of normally graded bedding of fine/medium sand. Red circles denote OSL age sampling locations with corresponding sample names and ages.

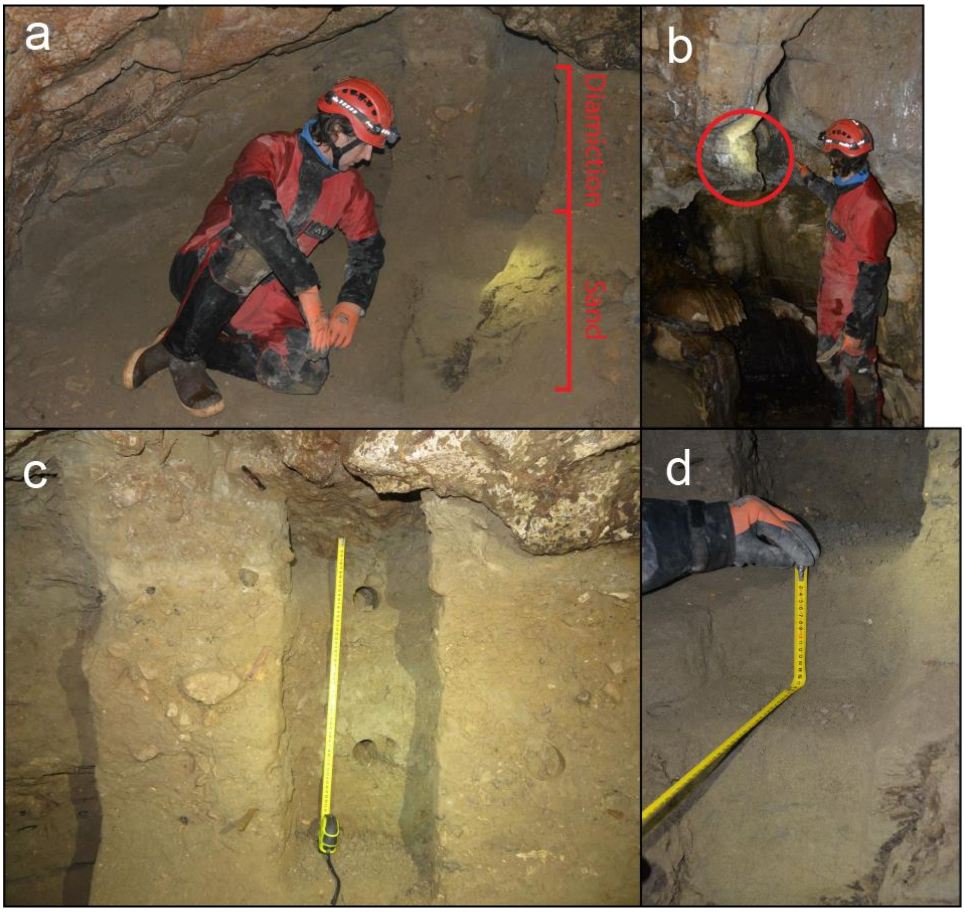

Extended Data Fig. 3: Images of DC Room and Devils Sequence. (**a**) Devils Sequence exposed with human for scale. (**b**) The possible former ice-sheet meltwater pathway in DC Room (red circle). (**c**) Selected segment of unit 1 composed of diamicton. (**d**) Selected segment of unit 2 composed of normally graded bedding of find/medium sand.

Extended Data Fig. 4: Images of Devils Canopy Cave surroundings. (**a**) Thickly vegetated temperate rainforest in the vicinity of Devils Canopy Cave with Entrance 1 (see Extended Data Fig. 1) located ~2 m to the left of people (red X). (**b**) Modern-day stream into Devils Canopy Cave (red X).

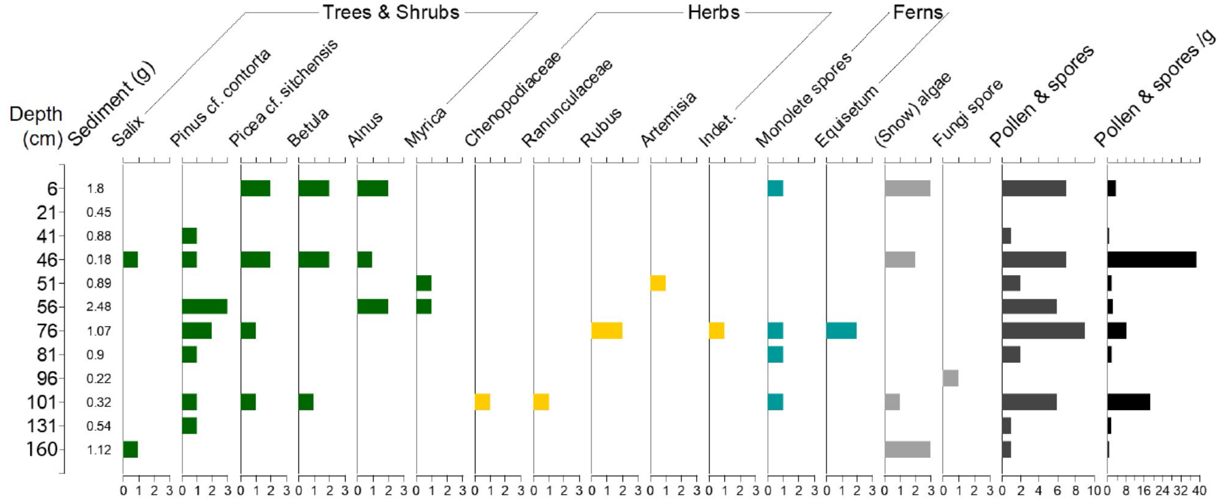

Extended Data Fig. 5: Pollen diagram of Devils Sequence. Absolute values of pollen, spores and algae are shown. Total pollen and fern spores concentration is shown in black.

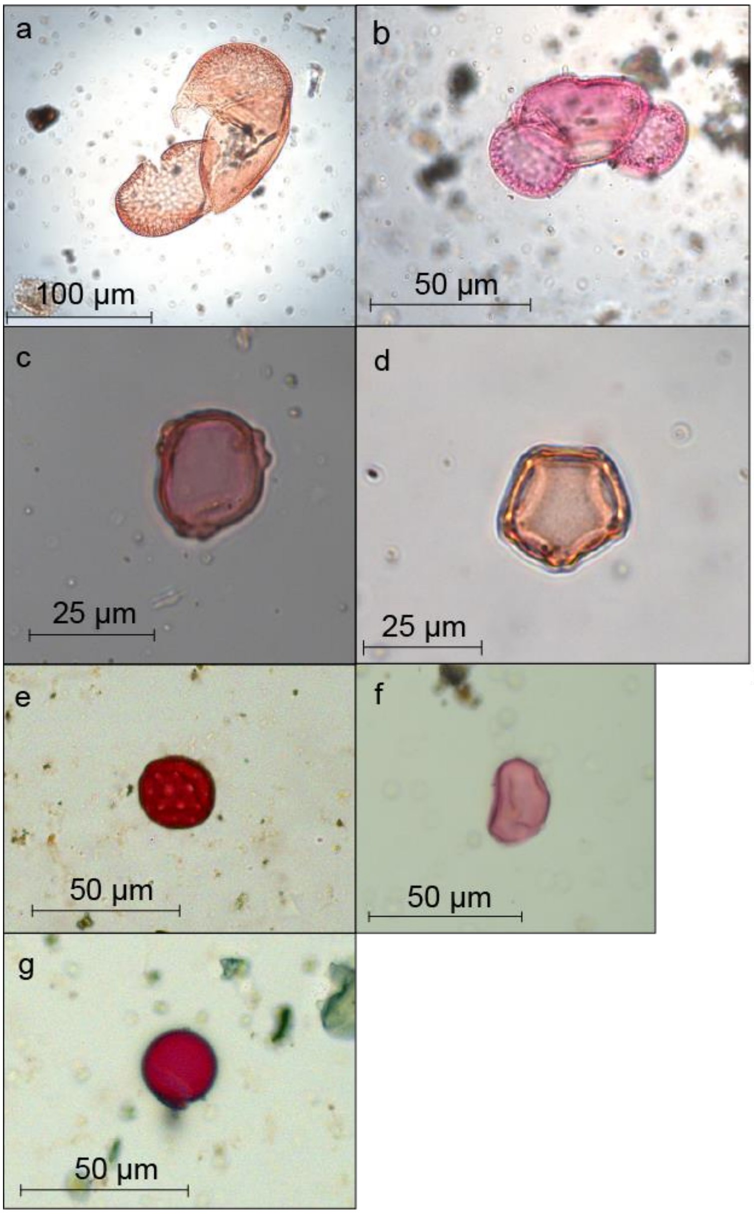

Extended Data Fig. 6: Examples of well-preserved microfossils found in the Devils Sequence: (**a**) *Picea* cf. *sitchensis*; (**b**) *Pinus* cf. *contorta*; (**c**) *Betula*; (**d**) *Alnus*; (**e**) Chenopodiaceae; (**f**) Fern monolete spore; (**g**) Algae (cf. snow algae).

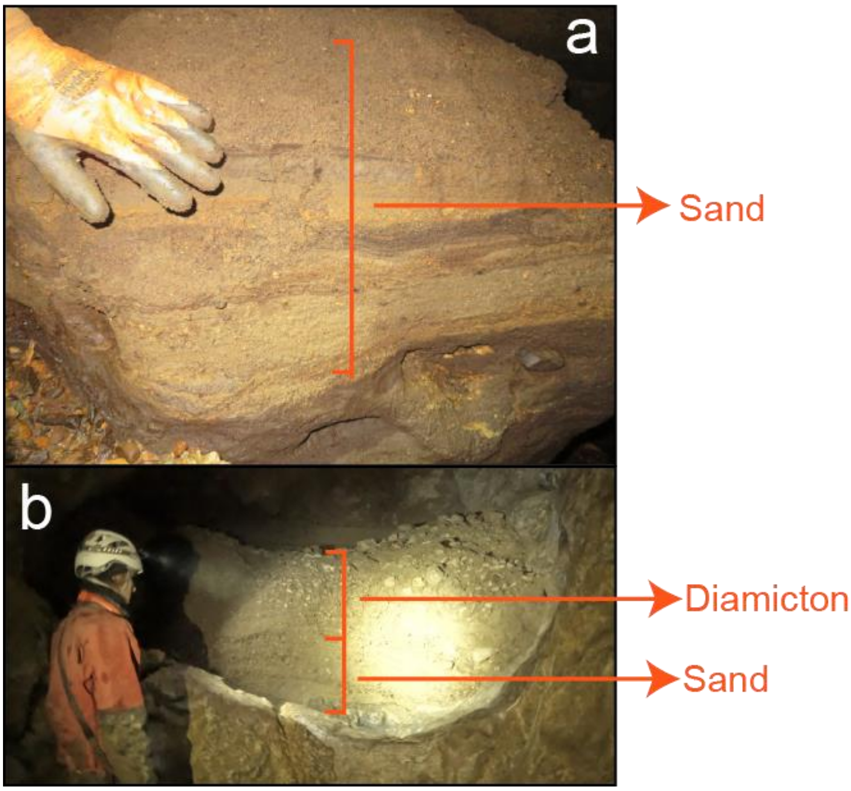

Extended Data Fig. 7: Sediments from other caves in the region showing similarities with Devils Sequence from Devils Canopy Cave. (**a**) Raven Cave, ~20 km northeast Devils Canopy Cave. (**b**) El Captain Cave, ~10 km northwest of Devils Canopy Cave (Fig. 1)

Extended Data Table 1: Dose rates, equivalent doses (De) and OSL ages for the Devils Canopy sediment samples based on minimum age model (MAM) solutions.

Sample name	Water content[1] (%)	Dose rate (Gy/ka)				aliquots accepted/ measured (n)	CAM De (Gy)	Over-dispersion (%)	MAM De (Gy)[3]	**MAM Age (ka)[4]**
		Beta	Gamma	Cosmic	Total[2]					
DCC1a	16.3	1.46 ± 0.07	0.76 ± 0.02	0.0008 ± 0.00	2.25 # 0.10	28/96	70.2 ± 7.3	48 ± 8	39.0 ± 6.9	**17.3 ± 3.0**
DCC2	13.3	1.64 ± 0.07	0.80 ± 0.02	0.0009 ± 0.00	2.48 ± 0.11	19/48	59.9 ± 7.4	43 ± 10	40.1 ± 4.6	**16.2 ± 2.0**
DCC4	11.6	1.44 ± 0.06	0.66 ± 0.01	0.0009 ± 0.00	2.03 ± 0.09	44/144	58.8 ± 4.3	38 ± 6	40.6 ± 5.8	**19.0 ± 2.9**

[1] For age calculation the field water content as measured for each sample has been used and an absolute error of 2.4% was added (i.e. STDE of field water content for all samples)

[2] Contains in internal quartz dose rate of 0.032±0.01 Gy/ka

[3] MAM 3-parameter model

[4] Age uncertainties are reported on the 2 sigma level

Extended Data Table 2: Radionuclide concentrations for the Devils Canopy Cave samples.

Sample name	Th (ppm)	U (ppm)	K (%)
DCC1a	2.100 ± 0.252	3.607 ± 0.073	1.512 ± 0.060
DCC2	4.264 ± 0.246	2.089 ± 0.071	1.849 ± 0.063
DCC4	2.719 ± 0.152	1.681 ± 0.044	1.633 ± 0.054

OSL DATING Supplementary Materials

Methods

Three OSL samples were collected by hammering 4-5 cm diameter opaque tubes into the cleaned Devils sedimentary sequence. Quartz grains of 150-180 mm diameter were extracted from the sediment samples in the laboratory under dim red illumination using standard procedures (Wintle, 1997; Murray et al., 2021). Hydrochloric acid (32%) and hydrogen peroxide (50%) were used to remove carbonates and organics, respectively. Sodium polytungstate solutions with densities of 2.70 g/cm^3 and 2.62 g/cm^3 were used to isolate quartz and feldspar grains from heavy minerals and quartz from feldspar grains, respectively. A hydrofluoric acid (40% for 40 min) etch was used to remove the external, alpha-dosed rind of the grains (Aitken, 1998) and contaminant feldspars. Finally, grains were rinsed in hydrochloric acid and sieved again to retain the target grain-size fraction. We were obtaining just enough material of sand-sized quartz from 3 out of 4 OSL tubes taken from the DCC sediment section for further OSL analysis.

Grains were loaded into a Risø DA20 TL/OSL reader (Bøtter-Jensen et al., 2003) and were measured using a post-IR blue protocol to ensure the purity of quartz OSL signals (Banerjee et al., 2001; Murray et al., 2021). Aliquots were stimulated with the Blue LEDs (470 ± 30 nm) following infrared (IR) (875 nm) stimulations. The blue as well as the IR LED clusters were operated at 90% power and were thus delivering approximately 36 mW/cm^2 and 122 mW/cm^2 to the sample position, respectively. The OSL signal was measured using an Electron Tubes Ltd 9635 photomultiplier tube and the ultraviolet emissions were measured through 7.5 mm of Hoya U-340 filter. IR stimulations were performed for 40 s at 50°C, and blue stimulations were performed for 100 s at 125°C.

Signals were integrated using an early-background subtraction approach (Cunningham and Wallinga, 2010) where the signal was summed between 0 and 1.6 s minus a background integrated between 1.6 and 4.8 s. Laboratory irradiations were given using a calibrated $^{90}Sr/^{90}Y$ beta source mounted on the Risø DA20 TL/OSL reader (dose rate of 0.097±0.001 Gy/s as per the 13.09.2023 based on Risø calibration quartz batch 90, grain size 180-212µm; corrected according to Autzen et al., 2022).

Small aliquots (1 mm diameter masks) were measured and equivalent dose (De) values were determined using the single-aliquot regenerative dose (SAR) procedure (Murray and Wintle, 2000). Dating attempts with even smaller sized aliquots were resulting in a significant drop in acceptable aliquots. This is likely due to the fact that Alaskan quartz has generally low sensitivity and only a small amount of sensitive grains exist per aliquot. Hence even 1mm aliquots probably approach pseudo-single-grain measurement level (Alexanderson and Murray, 2007; Duller, 2008). SAR measurements included regenerative dose preheats and test dose preheats, both at 180°C for 10 s. The appropriateness of the SAR procedure was assessed using standard tests, including (i) recycling ratio tests by repeating the regenerated dose points at 7 Gy (recycling ratio 1) and 88 Gy (recycling ratio 2), respectively, (ii) recuperation test (Murray and Wintle, 2000) and (iii) dose recovery tests (Roberts et al., 1999; Murray and Wintle, 2003).

The Central Age Model (CAM) and the Minimum Age Model (MAM; Galbraith et al., 1999; Galbraith and Roberts, 2012) were used to model De distributions and determine representative De values. For the MAM model 20% overdispersion (OD) were added as an input parameter before running the MAM and best fits were obtained with the 3-component MAM solution. This choice of the MAM OD value was based on the literature (e.g. Olley et al., 2004; Bailey and Arnold, 2006), rather than on OD values from dose recovery experiments, or on OD determinations from well-bleached analogue samples. It has to be pointed out that neither of these alternative ways of OD calculation for MAM modelling is per se superior over choosing a conservative 20% value from the literature, because (i) dose recovery experiments often tend to underestimate the true OD in a sample and this approach should thus be viewed with caution (Thomsen et al., 2005; Thomsen et al., 2012), (ii) our study was hampered by sample scarcity, hence the number of aliquots available for the dose recovery experiments (n=4 per preheat combination) is insufficient for robust calculation of OD values from our dose recovery experiments. OD value from the measurement of well-bleached analogue samples would have given valuable insights into the bleaching behaviour and thus the OD value of these sediments (Olley et al., 2004; Lomax et al., 2011), but none such (Pleistocene) analogue samples are available to us. Hence, a 20% OD from the literature is a conservative and well justified approach for our given setting.

The total environmental dose rate for each sample was measured using standard techniques. The results of beta counting using a GM-25-5 beta counter (Bøtter-Jensen and Mejdahl, 1988) and thick-source alpha counting and the conversion factors of Cresswell et al. (2018) were used to calculate beta and gamma dose rates (Extended Data Tables 1, 2). The cosmic-ray dose rate is, due to the large cave overburden and thus shielding, essentially negligible. An internal alpha dose rate of 0.03 ± 0.01 Gy/ka was assumed (Feathers et al., 2001; Jacobs et al., 2003). The measured field moisture content ranged from 10.8 to 16.3% and the average value with 1 sigma standard deviation is 13.0 ± 2.4%. For age calculation the measured field water content of each sample (as reported in Table 1) was used and a value of 2.4% (i.e. the standard deviation of the field water content for all samples) added as uncertainty. For dose rate attenuation in the age calculation the measured field water content with an error of ± 2.4% was used. Given that (i) the sediment was collected from deep inside the Devils Canopy Cave, (ii) the generally wet climate of Southern Alaska and (iii) the fact that inside a cave the cave air is generally at the saturation point, we exclude post depositional drying of the cave sediments. We further assume that no significant long-lasting sediment moisture fluctuations occurred over the sediment burial period and that any such fluctuations are covered by the relatively large error that we allowed for the measured field moisture content. As a general remark it is noted that any systematic change in sediment moisture content by 1% would shift the sediment burial age by ~1% in the same direction.

Results

Typical OSL decay curves and dose-response curves are shown in Figure 1 revealing that the OSL shine-down curves decay rapidly during the initial 3 to 4 seconds of optical stimulation but also reveal a more slowly decaying signal component thereafter and an elevated and slowly decaying background of ≥200 counts per channel for the rest of the optical stimulation. In addition, for some aliquots a moderate to low response to IR stimulation was observed, suggestive of a potential feldspar contamination, likely in the form of feldspar inclusions or quartz feldspar intergrowths (Meyer et al., 2013). Given the low amount of sample material and very low yield of quartz extract from these samples we opted for an optical IR wash in combination with an early background subtraction approach to remove any potential feldspar contributions to the blue OSL signal and isolate a fast-component dominated OSL signal. We deliberately refrained from an additional HF etching step because of sample scarcity, but opted for optically isolating a fast-component dominated OSL signal via a post-IR blue OSL approach (Banerjee et al., 2001). This approach has been introduced by Banerjee et al. in 2001 and has since then been extensively tested and successfully used for dating fine- as well as coarse-grained quartz extracts where feldspar contamination has been deemed to be of concern (e.g. Banerjee et al., 2001; Roberts and Wintle, 2001; Murray and Funder, 2003; Olley et al., 2004; Wang et al., 2006; Roberts, 2007; Roberts, 2008, Chapot et al., 2012). Importantly, these studies also confirmed that if the feldspar contribution to the OSL signal has already been reduced by etching, but cannot be removed completely via chemical treatments, the post-IR blue OSL approach is reliable in obtaining a fast-component dominated signal and an overall better alignment of the resulting post-IR blue OSL chronologies with expected age estimates is achieved (e.g. Murray and Funder, 2003; Olley et al., 2004; Wang et al., 2006; Roberts, 2007; Roberts, 2008, Chapot et al., 2012). Furthermore, in these studies no indication of a reduction of the intensity of the fast OSL component has been reported when using IR stimulation times between 40s and 200s, while in some instances IR stimulation times of up to 500s were successfully used too (e.g Wang et al., 2006).

Furthermore, we also tested a late background subtraction approach for sample DCC 2 using the SAR-based quality assurance criteria mentioned above and compared it with the early background approach (Fig. 2). We found that with late background subtraction (i) the number of acceptable aliquots dropped by more than 50% (from 19 to 9) mainly because of failing the recycling ratio and/or the recuperation criterion, (ii) the overdispersion increased from 43 to 63% and (iii) the error of the resulting CAM and MAM De values increased from 12 to 30%. Consequently, the error on the OSL age estimate also increased by a factor of 3. While the OSL age estimates of both background subtraction approaches for sample DCC 2 are identical within error, the loss in precision via late background subtraction is significant. It is concluded that the early background subtraction approach is preferably for our samples, presumably because it indeed removes a significant amount of medium and slow component contributions from the OSL signal integration interval, reduces the thermal transfer and thus recuperation as well as minimizes potential feldspar signal contributions, given that feldspar OSL decay is slower than quartz under 470 nm stimulation (Ballarini et al., 2007; Cunningham and Wallinga et al, 2010; Kars et al., 2012; Reimann et al., 2015; Yi et al., 2015). While Poisson background statistics are generally assumed for error calculation on the OSL decay curves it appears that this assumption – if violated via an early background subtraction – might be small in comparison to other effects and that, at least for the DCC samples, the combination of post-IR blue OSL dating and early background subtraction yields robust De estimates.

Dose recovery results conducted on sample DCC 3 yield measured/given dose ratios consistent with unity (1.08 ± 0.19). The average recycling ratios and the recuperation value for the 91 aliquots that were accepted from the three dating samples were 1.36 ± 1.35 (recycling ratio 1 at 7 Gy), 0.99 ± 0.34 (recycling ratio 2 at 88 Gy) and 3.02 ± 5.25 % for the recuperation test, respectively (reported with their respective standard deviations). These results indicate that the modified SAR procedure that is based on post-IR blue OSL approach in combination with an early background subtraction can accurately estimate known radiation doses for samples from Devils Canopy Cave. Equivalent dose, dose rate, and age data for all three OSL samples are shown in Table 1 and 2 of the SOM. Overdispersion values are 38 ± 7% for sample DCC 4 and 43 ± 11% and 48 ± 8% for samples DCC 2 and 1a, respectively. Well bleached samples typically show up to 20% overdispersion (Olley et al., 2004; Bailey and Arnold, 2006). Given the sedimentary context and poor sorting of samples DCC 1a and DCC 2, and DCC 4 and their high overdispersion values (i.e. well above 20%; Extended Data Table 1) we opted for a minimum age solution for the samples and subsequent age calculation (Galbraith et al., 1999; Olley et al., 2004; Fig. 2).

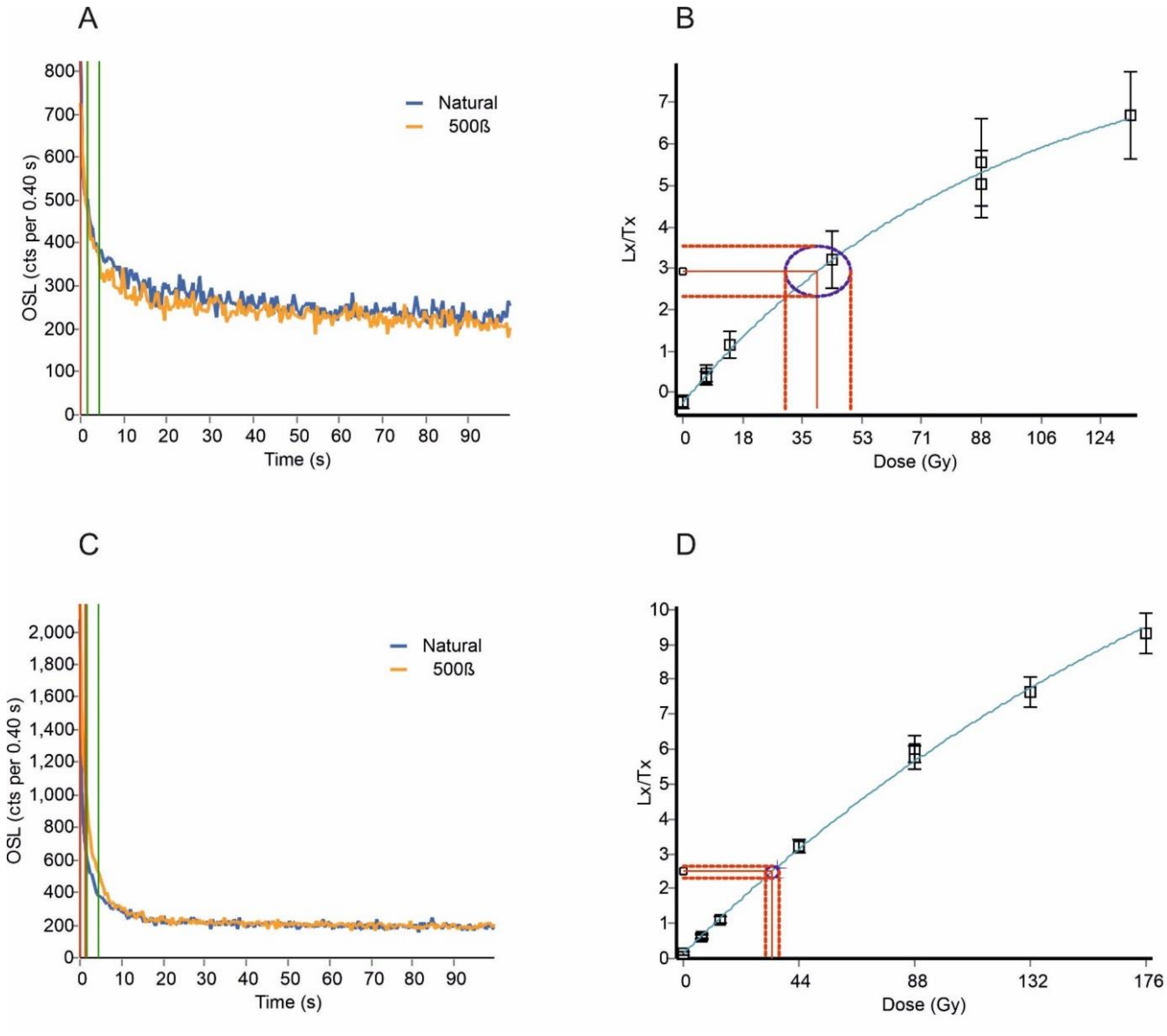

Figure 1: OSL Decay curves and SAR dose response curves for a typical dim (A, B) and a bright (C, D) aliquot from sample DCC 2. The error bars in B and D are based on the counting statistics of the background- and test dose-corrected natural and regenerated luminescence signals and calculated via the software Analyst (version 4.57; Duller 2007) following the approach outlined in Gailbraith 2002.

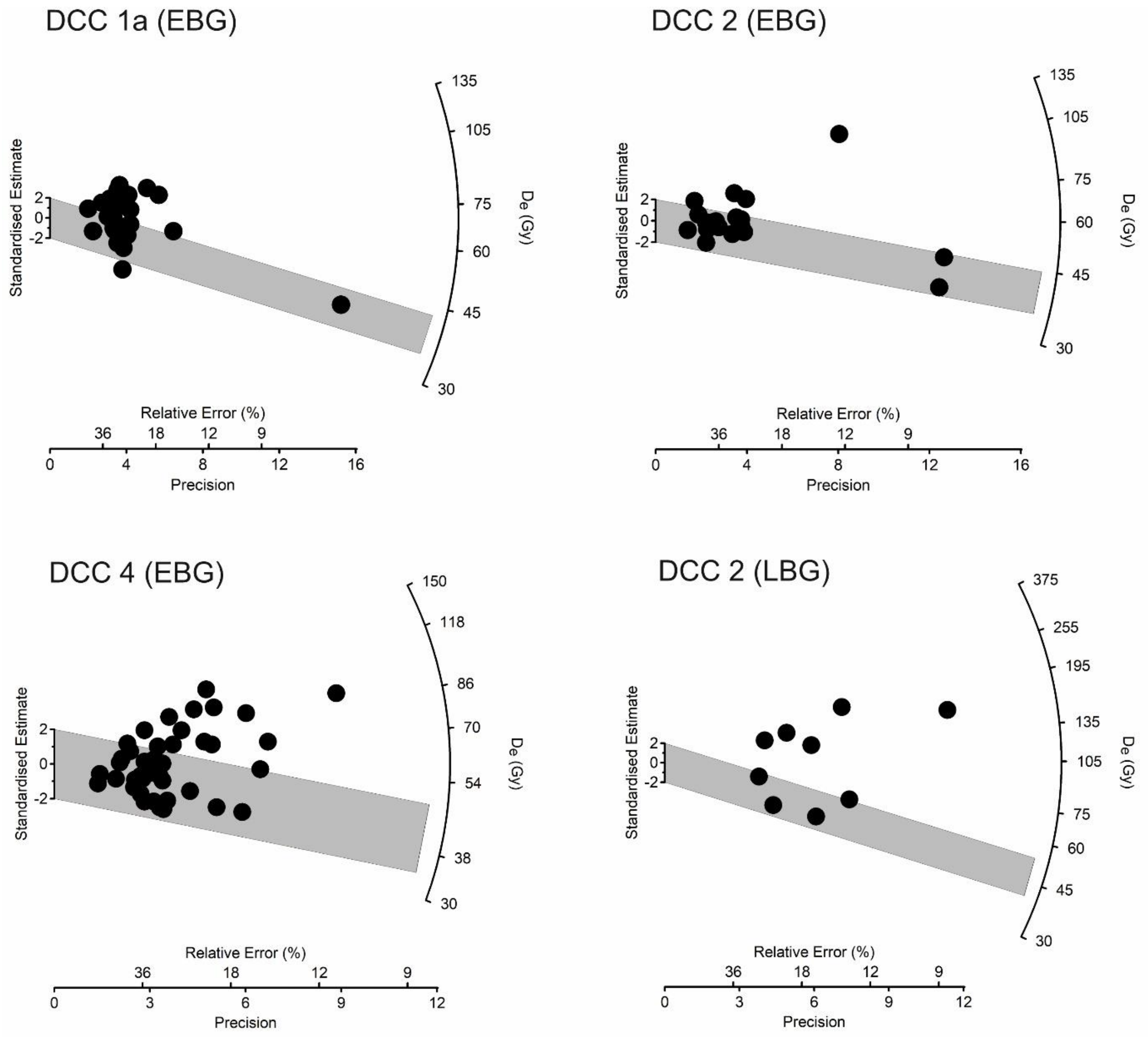

Figure 2: Radial plots showing De distributions for the three sediment samples from Devils Canopy Cave (DCC). Gray bar indicates MAM De value used for age calculation. For sample DCC 2 a direct comparison of the De distributions based on an early background (EBG) and a late background (LBG) subtraction approach, are shown. The EBG subtraction, and this background subtraction underpins the age calculation of all samples and the final MAM ages are shown in Table 1 of the main text.

References

Aitken, M.J., 1998. An Introduction to Optical Dating – the Dating of Quaternary Sediments by the Use of Photon-Stimulated Luminescence. Oxford University Press, Oxford.

Alexanderson, H., and Murray, A. S., 2007. Was southern Sweden ice free at 19–25 ka, or were the post LGM glacifluvial sediments incompletely bleached?. Quaternary Geochronology, v. 2, p. 229–236.

Autzen, M., Andersen, C., Bailey, M., Murray, A., 2022. Calibration quartz: an update on dose calculations for luminescence dating. Radiation Measurements 157, 106828.

Bailey, R.M., Arnold, L.J., 2006. Statistical modelling of single grain quartz De distributions and an assessment of procedures for estimating burial dose: Dating the Quaternary: progress in luminescence dating of sediments. Quaternary Science Reviews, v. 25, 2475–2502.

Ballarini, M., Wallinga, J., Wintle, A.G., Bos, A.J.J., 2007. A modified SAR protocol for optical dating of individual grains from young quartz samples. Radiation Measurements 42, 360-369.

Banerjee, D., Murray, A.S., Botter-Jensen, L., Lang, A., 2001. Equivalent dose estimation using a single aliquot of polymineral fine grains. Radiation Measurements, v. 33, p. 73–94.

Bøtter-Jensen, L., and Mejdahl, V., 1988. Assessment of beta dose-rate using a GM multicounter system: Nuclear Tracks Radiation Measurements, v. 14, p. 187–191.

Bøtter-Jensen, L., Andersen, C.E., Duller, G.A.T., and Murray, A.S., 2003. Developments in radiation, stimulation and observation facilities in luminescence measurements: Radiation Measurements, v. 37, p. 535–541.

Chapot, M.S., Roberts, H.M., Duller, G.A.T., Lai, Z.P., 2012. A comparison of natural- and laboratory-generated dose response curves for quartz optically stimulated luminescence signals from Chinese Loess. Radiation Measurements 47, 1045-1052.

Cresswell, A.J., Carter, J., Sanderson, D.C.W., 2018. Dose rate conversion parameters: Assessment of nuclear data. Radiation Measurements, v. 120, p. 195-201.

Cunningham, A.C., and Wallinga, J., 2010. Selection of integration time intervals for quartz OSL decay curves: Quaternary Geochronology, v. 5, p. 657–666.

Cunningham, A.C., Wallinga, J., 2010. Selection of integration time intervals for quartz OSL decay curves. Quaternary Geochronology 5, 657-666.

Duller, G.A.T., 2007. Assessing the error on equivalent dose estimates derived from single aliquot regenerative dose measurements. Ancient TL 25, 15-23.

Duller, G. A., 2008. Single-grain optical dating of Quaternary sediments: why aliquot size matters in luminescence dating. Boreas, v. 37, p. 589-612.

Feathers, J.K., Migliorini, E., 2001. Luminescence dating at Katanda e a reassessment. Quaternary Science Reviews, v. 20, p. 961–966.

Galbraith, R.F., Roberts, R.G., Laslett, G.M., Yoshida, H., and Olley, J.M., 1999. Optical dating of single and multiple grains of quartz from Jinmium rock shelter, northern

Australia: part I, experimental design and statistical models: Archaeometry, v. 41, p. 339–364.

Galbraith, R., 2002. A note on the variance of a background corrected OSL count. Ancient TL 20, 49-52.

Galbraith, R.F., and Roberts, R.G., 2012. Statistical aspects of equivalent dose and error calculation and display in OSL dating: an overview and some recommendations: Quaternary Geochronology, v. 11, p. 1–27.

Jacobs, Z., Wintle, A.G., Duller, G.A.T., 2003. Optical dating of dune sand from Blombos Cave, South Africa: I e multiple grain data. Journal of Human Evolution, v. 44, p. 599–612.

Kars, R., Busschers, F., Wallinga, J., 2012. Validating post IR-IRSL dating on K-feldspars through comparison with quartz OSL ages. Quaternary Geochronology 12, 74-86.

Lomax, J., Hilgers, A. & Radtke, U. Palaeoenvironmental change recorded in the palaeodunefields of the western Murray Basin, South Australia – New data from single grain OSL-dating. Quaternary Science Reviews 30, 723-736 (2011).

Meyer, M.C., Austin, P., Tropper, P., 2013. Quantitative evaluation of mineral grains using automated SEM-EDS analysis and its application potential in optically stimulated luminescence dating. Radiation Measurements, v. 58, p. 1–11.

Murray, A., Arnold, L.J., Buylaert, J.-P., Guérin, G., Qin, J., Singhvi, A.K., Smedley, R., Thomsen, K.J., 2021. Optically stimulated luminescence dating using quartz. Nature Reviews Methods Primers, v. 1, p. 1–31.

Murray, A.S., and Wintle, A.G., 2000. Luminescence dating of quartz using an improved single- aliquot regenerative-dose protocol: Radiation Measurements, v. 32, p. 57–73.

Murray, A.S., and Wintle, A.G., 2003. The single aliquot regenerative dose protocol: potential for improvements in reliability: Radiation Measurements, v. 37, p. 377–381.

Murray, A.S., Funder, S., 2003. Optically stimulated luminescence dating of a Danish Eemian coastal marine deposit: a test of accuracy: LED 2002. Quaternary Science Reviews 22, 1177-1183.

Olley, J.M., Pietsch, T., Roberts, R.G., 2004. Optical dating of Holocene sediments from variety of geomorphic settings using single grains of quartz. Geomorphology, v. 60, p. 337–358.

Reimann, T., Notenboom, P.D., De Schipper, M.A., Wallinga, J., 2015. Testing for sufficient signal resetting during sediment transport using a polymineral multiple-signal luminescence approach. Quaternary Geochronology 25, 26-36.

Roberts, H.M., 2007. Assessing the effectiveness of the double-SAR protocol in isolating a luminescence signal dominated by quartz. Radiation measurements 42, 1627-1636.

Roberts, H.M., 2008. The development and application of luminescence dating to loess deposits: a perspective on the past, present and future. Boreas 37, 483-507.

Roberts, H.M., Wintle, A.G., 2001. Equivalent dose determinations for polymineralic fine-grains using the SAR protocol: application to a Holocene sequence of the Chinese Loess Plateau. Quaternary Science Reviews 20, 859-863.

Roberts, R.G., Galbraith, R.F., Olley, J.M., Yoshida, H., and Laslett, G.M., 1999. Optical dating of single and multiple grains of quartz from Jinmium rock shelter, northern Australia: part II, results and implications: Archaeometry, v. 41, p. 365–395.

Thomsen, K. J., Murray, A. & Jain, M. The dose dependency of the over-dispersion of quartz OSL single grain dose distributions. Radiation Measurements 47, 732-739 (2012).

Thomsen, K. J., Murray, A. S. & Bøtter-Jensen, L. Sources of variability in OSL dose measurements using single grains of quartz. Radiation Measurements 39, 47-61 (2005).

Wang, X., Lu, Y., Zhao, H., 2006. On the performances of the single-aliquot regenerative-dose (SAR) protocol for Chinese loess: fine quartz and polymineral grains. Radiation Measurements 41, 1-8.

Wintle, A.G., 1997. Luminescence dating: laboratory procedures and protocols: Radiation Measurements, v. 27, p. 760–817.

Yi, S., Buylaert, J.-P., Murray, A.S., Thiel, C., Zeng, L., Lu, H., 2015. High resolution OSL and post-IR IRSL dating of the last interglacial–glacial cycle at the Sanbahuo loess site (northeastern China). Quaternary Geochronology 30, 200-206.